Journal of Nuclear Materials 406 (2010) 218–222

Contents lists available at ScienceDirect

Journal of Nuclear Materials

journal homepage: www.elsevier.com/locate/jnucmat

Structural, electronic, and thermodynamic properties of UN: Systematic density functional calculations

Yong Lu [a,b], Bao-Tian Wang [b,c], Rong-Wu Li [a], Hongliang Shi [b], Ping Zhang [b,d,*]

[a] Department of Physics, Beijing Normal University, 100875, People's Republic of China
[b] LCP, Institute of Applied Physics and Computational Mathematics, Beijing 100088, People's Republic of China
[c] Institute of Theoretical Physics and Department of Physics, Shanxi University, Taiyuan 030006, People's Republic of China
[d] Center for Applied Physics and Technology, Peking University, Beijing 100871, People's Republic of China

ARTICLE INFO

Article history:
Received 31 May 2010
Accepted 24 August 2010

ABSTRACT

A systematic first-principle study is performed to calculate the lattice parameters, electronic structure, and thermodynamic properties of UN using the local-density approximation (LDA)+*U* and the generalized gradient approximation (GGA)+*U* formalisms. To properly describe the strong correlation in the U 5*f* electrons, we optimized the *U* parameter in calculating the total energy, lattice parameters, and bulk modulus at the nonmagnetic (NM), ferromagnetic (FM), and antiferromagnetic (AFM) configurations. Our results show that by choosing the Hubbard *U* around 2 eV within the GGA+*U* approach, it is promising to correctly and consistently describe the above mentioned properties of UN. The localization behavior of 5*f* electrons is found to be stronger than that of UC and our electronic analysis indicates that the effective charge of UN can be represented as $U^{1.71+}N^{1.71-}$. As for the thermodynamic study, the phonon dispersion illustrates the stability of UN and we further predict the lattice vibration energy, thermal expansion, and specific heat by utilizing the quasiharmonic approximation. Our calculated specific heat is well consistent with experiments.

1. Introduction

Uranium nitrides have been extensively studied in experiments in connection with their potential applications in the Generation-IV reactors [1]. These reactors raise a number of concerns surrounding the issue of nuclear energy. The fission reactions depend on fast neutrons, requiring a small core with a high power density and very efficient heat transfer. The oxide based fuels are therefore being involved in the ongoing research and development, however, the nitride fuels also participate in the competition to become the alternative materials for their superior thermal physical properties, such as high melting point, high thermal conductivity, and high metal density [2], as well as the good compatibility with the coolant (Na). On account of these obvious importances, several studies, such as electronic structures [3,4], surface properties [5], magnetic properties [6], point defects [7], and elastic constants [8], have already been conducted for uranium nitride, as well as systematic calculations for a series of actinide nitrides [9,10].

It is well known that conventional density functional theory (DFT) which apply the LDA or GGA underestimates the strong on-site Coulomb repulsion of the 5*f*-electron and, consequently, describes UN as incorrect FM conductor instead of the experimentally observed AFM type-I structure [11] at the Néel temperature T_N = 53 K. Similar problems have been confirmed in studying other electronically correlated materials within the pure LDA/GGA scheme. In the present work, we use the LDA/GGA+*U* method developed by Dudarev et al. [12] to effectively remedy the failures raised by LDA/GGA in describing the strong intra-atomic Coulomb interaction. This method has been successfully used to study the correlated problems [13–15].

In this paper, we have systematically calculated the lattice parameters, electronic structure, as well as the thermodynamic properties of UN using the above mentioned LDA/GGA+*U* scheme. We have carefully discussed how these properties are affected by the choice of *U* as well as the choice of exchange-correlation potential. After testing the validity of the ground state by choosing *U* around 2 eV within the GGA+*U* approach, we performed a series of calculations on the electronic structures, bonding properties, and the phonon dispersion. The lattice vibration energy, thermal expansion, and specific heat were obtained by utilizing the quasiharmonic approximation (QHA) based on the first-principles phonon density of state (DOS). The rest of the paper is organized as follows. The computational details of first-principles are briefly introduced in Section 2. The calculation results are presented and discussed in Section 3. Finally, we give a summary of this work in Section 4.

* Corresponding author. Tel.: +86 10 82305133.
E-mail address: zhang_ping@iapcm.ac.cn (P. Zhang).

0022-3115/$ - see front matter © 2010 Elsevier B.V. All rights reserved.
doi:10.1016/j.jnucmat.2010.08.026

2. Computational methods

The DFT total energy calculations were carried out using the Vienna *ab initio* simulations package (VASP) [16,17] with the projected-augmented-wave (PAW) pseudopotentials [18] and plane waves. The exchange and correlation effects were described within LDA and GGA [19,20]. The uranium $6s^26p^66d^25f^27s^2$ and nitrogen $2s^22p^3$ electrons were treated as valence electrons. The electron wave function was expanded in plane waves up to a cutoff energy of 500 eV. We have performed numerous convergence studies on determining the influence on the total energy of the *k*-point mesh. The Monkhorst-Pack [21] $9 \times 9 \times 9$ mesh (75 irreducible *k* points) in Brillouin zone (BZ) integration was sufficient to get results converged to less than 1.0×10^{-4} eV per atom and the corresponding electronic DOS was obtained with $15 \times 15 \times 15$ (120 irreducible *k* points) *k*-point mesh.

As mentioned above, the strong on-site Coulomb repulsion among the localized U 5*f* electrons were described by using the formalism developed by Dudarev et al. [12] and the total LDA/GGA+*U* energy functional is of the form:

$$E_{\mathrm{LDA(GGA)+U}} = E_{\mathrm{LDA(GGA)}} + \frac{U-J}{2}\sum_{\sigma}[\mathrm{Tr}\rho^{\sigma} - Tr(\rho^{\sigma}\rho^{\sigma})],$$

where ρ^{σ} is the density matrix of *f* states with spin σ, while *U* and *J* are the spherically averaged screened Coulomb energy and the exchange energy, respectively. This can be understood as adding a penalty functional to the LDA/GGA total energy expression that forces the on-site occupancy matrix in the direction of idempotency. However, the use of the LDA/GGA+*U* approximation induces an increase in the number of metastable states which makes the convergence to the ground state difficult [22]. Consequently, different starting points of the calculation will lead to the discrepancy of final state reached by the self-consistent algorithm and its associated total energy. While this problem can be solved by performing a procedure, which is based on the monitoring of the occupation matrices of the correlated orbitals. Such a procedure can unequivocally determines the ground state by comparing the energies of all energy minima, as presented by Jomard et al. [23] and Dorado et al. [24]. In this expression, the total energy will depend on the difference between parameters *U* and *J*. Therefore the parameters *U* and *J* do not enter separately and only the difference (*U*–*J*) is meaningful. In this paper, the Coulomb parameter *U* is treated as one variable, and we will perform numerous studies and comparison to determine its value. While the exchange parameter *J* is set to 0.51 eV for U atom. This value is the same as that determined by Dorado et al. [24], and close to that determined by Kotani et al. [25] who made a systematic analysis of core levels X-ray photoemission spectra using the Anderson-impurity model. Since only the difference between *U* and *J* is meaningful in Dudarev's approach, therefore, we label them as one single parameter *U* for simplicity.

3. Results and discussions

3.1. Atomic and electronic structures of UN

We study UN in its ground state NaCl-type ($Fm\bar{3}m$) structure. In the present LDA/GGA+*U* approach, we have considered the NM, FM, and AFM phases for each choice of the value of *U*, and determined the ground state phase by a subsequent total energy comparison of these three phases. Compared with the FM and AFM phases, the NM phase is not energetically favorable both in the LDA+*U* and GGA+*U* formalisms. Therefore, the results of NM are not presented in the following. The dependence of the total energies (per formula unit) for UN in both AFM and FM configurations on *U* are shown in Fig. 1. At $U = 0$ eV, the ground state of UN is determined to be a FM metal, which is in contrast to experiment results. By increasing the amplitude of *U*, our LDA/GGA+*U* calculation correctly predicts an AFM metal ground state and the turning value of *U* is ~1.5 eV and ~2 eV in GGA+*U* and LDA+*U* approaches, respectively. In the discussion that follows, we, therefore, confine our report to the AFM phase of UN.

In this paper, the theoretical equilibrium volume V_0, bulk modulus *B* are obtained by fitting the third-order Birch–Murnaghan equation of state (EOS) [26]. Our calculated lattice parameter a_0 and *B* for the cubic unit cells of UN are shown in Fig. 2. For the pure DFT calculations ($U = 0$ eV), both the LDA and GGA methods underestimate the lattice parameter with respect to the experimental value. This trend is more evident for LDA approach due to its over-binding character. After turning on the Hubbard parameter *U*, the value of a_0 gradually improves for both LDA and GGA approaches. At around $U = 1$–2 eV, the GGA+*U* gives $a_0 = 4.896$–4.926 Å, which consists well with the experimental data [7] of $a_0 = 4.886$ Å, within 1% error. And this value is somewhat larger than other theoretical results 4.83 Å (LMTO) in Ref. [3] and 4.80 Å (LCAO-SC60) in Ref. [5]. Within LDA+*U*, the lattice constant can be satisfied by turning on the Hubbard *U* parameter at around 4 eV. We observe that the tetragonal distortion associated with AFM order of this type is rather small, i.e., $|c/a - 1| = 0.0239$, which is somewhat larger than the measured value of 6.5×10^{-4} at 4.2 K by Maples et al. [27].

The dependence of bulk modulus *B* on *U* is presented in Fig. 2b. It is clear that the LDA+*U* results are always higher than that from GGA+*U*. This is due to above mentioned over-binding effect of the LDA approach. With increasing the amplitude of *U*, the value of *B* shows a clear declining trend for both schemes. For AFM phase, the GGA results show that the variety of *B* is small in the range of $U = 2$–5 eV . At $U = 2$ eV, the value of *B* equals to 194.5 GPa, which coincides well with the experimental data (194 GPa in Ref. [28], 200 GPa in Ref. [8], and 206 GPa in Ref. [29]). The LDA results always hold higher *B* values than experimental data till the amplitude of *U* over 4 eV. The calculated value of magnetic moment increases from 0.90 μ_B to 1.57 μ_B (per uranium atom) by turning on the Hubbard *U* from 0 eV to 2 eV within GGA+*U* formalism, going towards the neutron spectroscopy value of 2.5 μ_B which was measured by Holden et al. [30]. Although it can be improved by including spin-orbit coupling (SOC), the amplitude is relatively small. The SOC, which can be important for certain properties of heavy metal compounds, is neglected in our present study, since our main purpose is not to give a quantitative estimation of the SOC effect. On the whole, considering the magnetic configurations, the GGA+*U* can give a satisfactory prediction of ground state atomic structures and bulk modulus *B* by tuning *U* to be near 2 eV for UN.

Besides the above effect of LDA/GGA+*U* on the atomic structure parameters, in the following discussion we further systematically

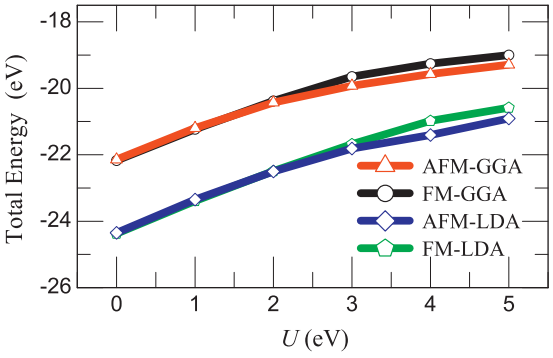

Fig. 1. Dependence of the total energies (per formula unit) on U for FM and AFM UN.

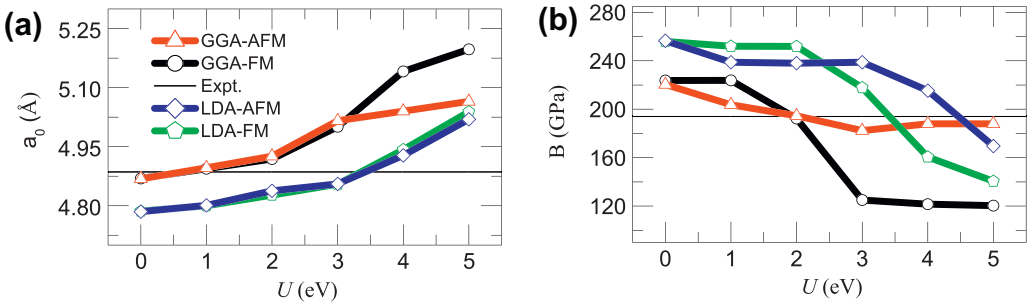

Fig. 2. Dependence of the equilibrium lattice parameter a_0 (a) and the bulk modulus B (b) on U.

investigate the electronic structures within the two theoretical treatments. The total electronic DOS together with the orbital-resolved site-projected DOS (PDOS) of UN are displayed in Fig. 3. Evidently, a large degree of U d–f orbitals can be observed in the valence band near the Fermi level, and the conduction band is strongly marked by f orbitals. The p orbitals play a great role in the valence band, with some degree of hybridization with d orbitals. Under the SIC-LSD calculations in Ref. [10], the localized and delocalized f-electron configurations were discussed, which indicate that the f^1 is the energetically favorable configuration. However, it still remains unclear whether a localized, delocalized, or dual localized/delocalized picture can best account for the experimentally observed properties of UN. It is only certain that the localization in UN is stronger than that in UC [15,10]. For UC, one part of the 5f electrons transfer into the interstitial zone, the other part are expected to be confined to the $j = 5/2$ multiplet, and the itineracy of 5f electrons are evident. Similar to UC, for UN, as the increase of the Hubbard parameter U, the itineracy of the 5f electrons still exists in UN. At a typical value of $U = 2$ eV, the conduction band f-electron occupancy is ~2.44 electrons, compared well with the 2.2 ± 0.5 electrons measured by Norton et al. [31] using the photoelectron-spectroscopic method. Due to the strong overlap of the U 5f orbitals near the Fermi energy, the UN phase exhibits a clear metallic behavior.

In order to further analyze the chemical bonding nature of UN, we present in Fig. 4 the charge density map of the (0 0 1) plane for AFM phase of UN with $U = 2$ eV in GGA formalism. It is evident that the charge density around U and N ions are all near spherical distribution with slightly deformed toward the direction to their nearest neighboring atoms. There are clear covalent bridges between U and N ions. For the sake of describing the ionic/covalent character quantitatively, we calculate the effective Bader charges [32]. We adopt 336 × 336 × 336 charge density grids. The calculated valance charges are listed in Table 1 together with the LCAO (Ref. [4]) and PW91 (Ref. [33]) results for comparison. Our present Bader analysis gives the valency of $U^{1.71+}N^{1.71-}$, in qualitative agreement with the LCAO ($U^{1.58+}N^{1.58-}$) and PW91 ($U^{1.66+}N^{1.66-}$) results. All the data and analysis confirm the conclusion that the bonding of U–N in UN compound is essentially covalent.

3.2. Phonon dispersion curve of UN

Through the above discuss on atomic and electronic structures on U, we choose the GGA+U approach with the Hubbard $U = 2$ eV to calculate the phonon dispersions for UN. In calculating the phonon dispersion curves and the phonon density of states, the Hellmann-Feynman theorem and the direct method [34] are employed. For the BZ integration, the 3 × 3 × 3 Monkhorst-Pack k-point mesh is used for the 2 × 2 × 2 UN supercell containing 64 atoms. In order to calculate the Hellmann-Feynman forces, we displace two atoms (one U and one N atoms) from their equilibrium positions and the amplitude of all the displacements is 0.03 Å. Besides, we have calculated the Born effective charges of UN for their critical importance in correcting the LO–TO splitting. Because of its high symmetry for UN, the off-diagonal elements of the Born effective charge tensor are all zero and the three diag-

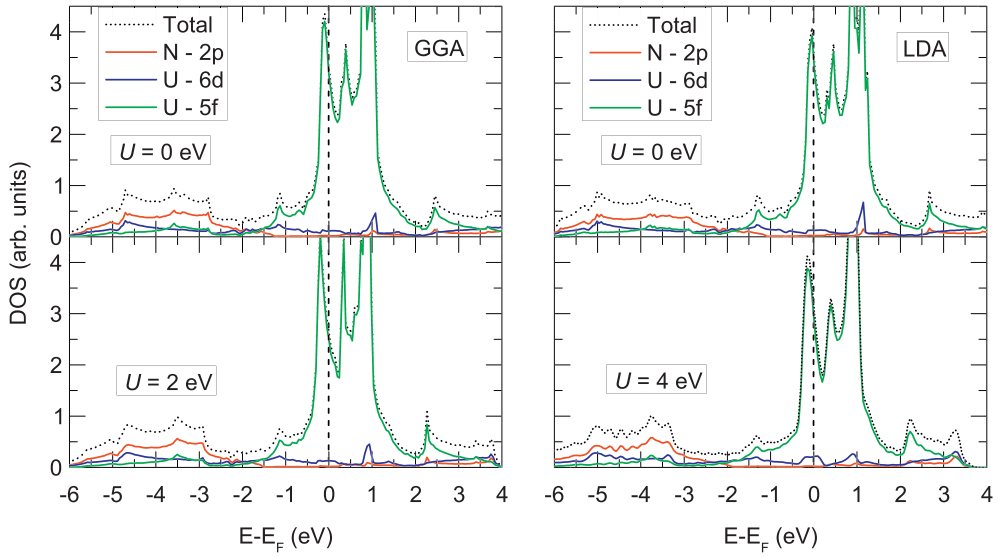

Fig. 3. The total DOS for the UN AFM phase computed in the GGA, GGA+U ($U = 2$), LDA, and LDA+U ($U = 4$) formalisms. The projected DOSs for the U 5f/6d and N 2p orbitals are also shown. The Fermi energy level is set at zero.

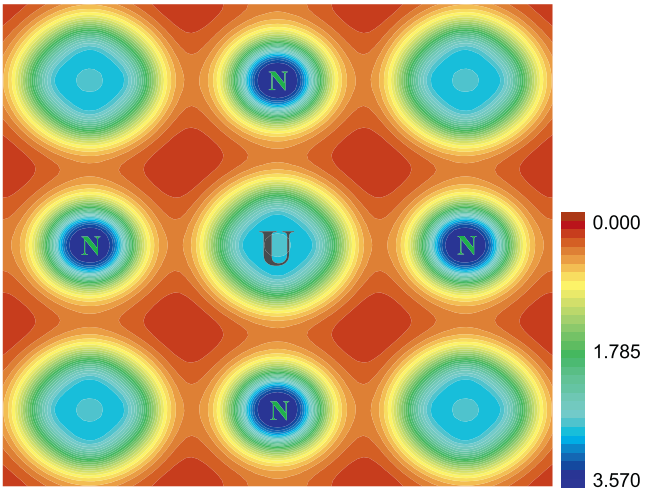

Fig. 4. Valence charge density of UN (001) plane within GGA+U approach at U = 2 eV.

Table 1
Bader effective atomic charges of UN. The calculated results using LCAO (Ref. [4]) and PW91 (Ref. [33]) methods are also listed for comparison.

Methods	Bader charge	UN
GGA+U	Q_U	+1.71
	Q_N	−1.71
LCAO	Q_U	+1.58
	Q_N	−1.58
PW91	Q_U	+1.66
	Q_N	−1.66

onal elements Z_{xx}, Z_{yy} and Z_{zz} are the same. Therefore, only Z_{xx} is shown here. Our calculated results for UN are $Z^*_U = +1.95$ and $Z^*_N = -1.95$. The calculated phonon dispersion curves along $\Gamma - X - K - \Gamma - L$ directions is displayed in Fig. 5. The experimental data from Ref. [35] (at T = 4.2 K) are also presented for comparison. For NaCl-type UN, there are only two atoms in its formula unit, therefore, six phonon modes exist in the dispersion relations. As shown in Fig. 5, our calculated LA/TA branch is in good agreement with experiment. The remarkable splitting between LO and TO at Γ point can be attributed to the inclusion of the Born effective charges in our phonon dispersion calculation. The TO frequency at Γ point is 12.19 THz. This result is well consistent with the available experimental value of 12.3 THz at 4.2 K. In addition, the phonon DOS splits into two parts with one part in range of 0–4.7 THz where the vibrations of uranium atoms are dominant and another part in the domain of 10.5–15 THz where the vibrations mainly come from nitride atoms. This evident gap between the optic modes and the acoustic branches is because of the fact that the uranium atom is heavier than nitride atom. In the following discussions, the reliability of the phonon dispersion calculation will give an accuracy evaluation of the thermodynamic properties.

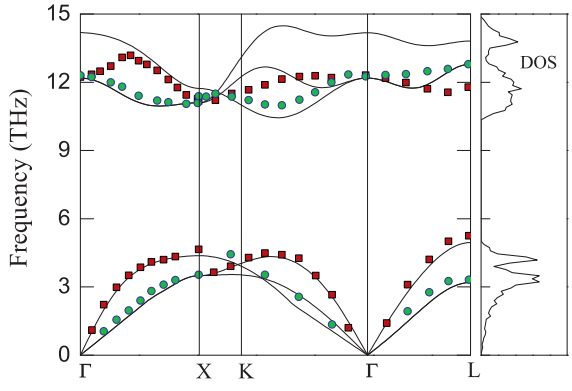

Fig. 5. Calculated phonon dispersion curves (left panel) and corresponding DOS (right panel) within GGA+U approach at U = 2 eV for AFM UN.

3.3. Thermodynamic properties

To calculate thermodynamical quantities such as the lattice vibration energy, thermal expansion, and specific heat, the Helmholtz free energy F in QHA is investigated as follows:

$$F(V,T) = E(V) + F_{ph}(V,T) + F_{ele}(V,T), \tag{1}$$

where $E(V)$ stands for the ground state energy, $F_{ph}(V,T)$ is the phonon free energy at a given unit cell volume V, and F_{ele} is electron excitation energy. Under QHA, the $F_{ph}(V,T)$ can be calculated from phonon DOS by

$$F_{\mathrm{ph}}(V,T) = k_{\mathrm{B}}T\int_0^\infty g(\omega)\ln\left[2sinh\left(\frac{\hbar\omega}{2k_BT}\right)\right]d\omega, \tag{2}$$

where $\omega = \omega(V)$ denotes the volume-dependent phonon frequencies, $g(\omega)$ is the phonon density of states, $\hbar$ is the Planck constant, and k_B is the Boltzmann constant. Eq. (2) contains some effect of unharmonics since the phonon frequencies have to be derived each time at the current crystal volume V. In addition, the specific heat for constant volume C_V can be obtained directly as

$$C_V = \left(\frac{\partial F}{\partial T}\right)_V = k_{\mathrm{B}}\int_0 d\omega g(\omega)\left(\frac{\hbar\omega}{k_{\mathrm{B}}T}\right)^2\frac{exp(\frac{\hbar\omega}{k_{\mathrm{B}}T})}{\left[exp\left(\frac{\hbar\omega}{k_{\mathrm{B}}T}\right)-1\right]^2}. \tag{3}$$

Then the specific heat at constant pressure C_P is given by

$$C_P - C_V = \alpha_V^2(T)B(T)V(T)T, \tag{4}$$

where the constant volume thermal expansion α_V is defined by $\alpha_V = \frac{1}{V}\left(\frac{\partial V}{\partial T}\right)_P$. The electronic excitation effect on the specific heat is accounted by the free-electron Fermi gas model, $C_e = \gamma T_e$, where γ is the electronic specific heat coefficient. For noninteracting electrons, the value of γ is reasonable at low electron temperature (T_e < 3000 K). It is proportional to the total density of states $N(E_F)$ at the Fermi level and is given by $\frac{\pi^2}{3}k_B^2N(E_F)$.

In our calculations, the unit cell volume is varied to a set of value. The calculated free energy versus volume curves for a number of selected temperatures is plotted in Fig. 6, from which the volume expansion upon the temperature increase can be derived. The calculated heat capacity C_P of UN is displayed in Fig. 7. For comparison, the experimental data from Refs. [36–41] and the theoretical results by Chevalier et al. (N–U modelling calculation) [42] and Weck et al. [43] (all-electron calculation) are also presented. As shown in Fig. 7, on the whole, the calculated thermodynamic function with no electronic excitation contribution is lower than the experimental ones. Furthermore, as the T increasing (T > 100 K), the discrepancy is enlarged gradually. This kind of underestimation in the high temperature domain has also been observed in the all-electron calculation [43]. Therefore, one needs to take into account the conduction electrons contributions to the C_P for metallic material UN. Our estimated value for the electronic specific heat coefficient γ is equal to 26.7 mJ K^{-2} mol^{-1}, which is somewhat lower than the experimental value of 49.6 mJ K^{-2} mol^{-1} [30]. The reason can be mainly attributed to the ignorable electron–phonon interactions and many body effects. In the future work, we will pursue such studies. The specific heat capacity including electronic

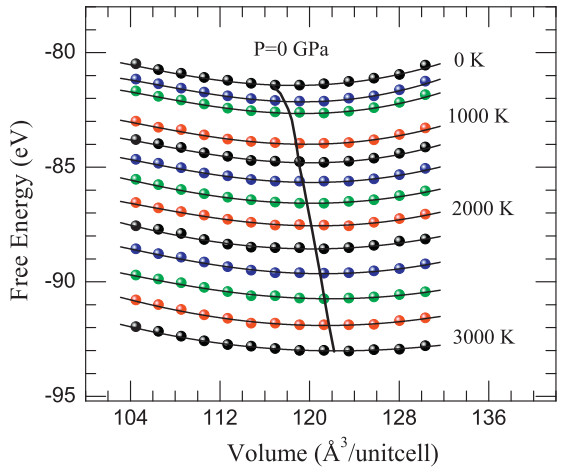

Fig. 6. Dependence of the Helmholtz free energy $F(T,V)$ on crystal volume at various temperatures. The locus of the minimum of the free energy for UN is also presented.

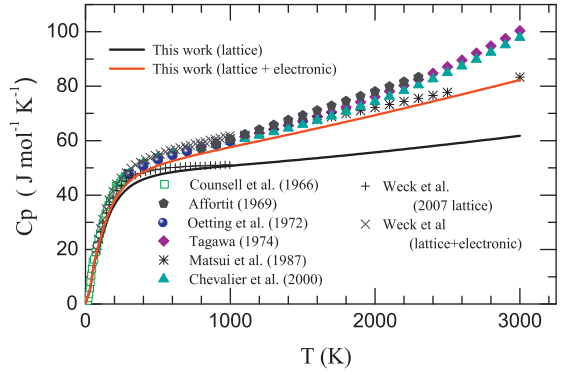

Fig. 7. Heat capacity of UN calculated within GGA+U at $U = 2$ eV with and without considering the contribution of electrons. Experimental data from Refs. [36–41] and theoretical results from Refs. [42,43] are also displayed for comparison.

contribution is also displayed in Fig. 7. One can see that the C_P with electronic corrections is largely enhanced, approaching to the experimental value. The C_P at low temperature ($T < 150$ K) is in good agreement with the experimental data. While at the $T > 150$ K region, it is still somewhat lower than the experimental value. The reason might be that the UN compound is not AFM anymore (as $T_N = 53$ K), while we still consider the AFM, which affects the electronic contribution (different $N(E_F)$) to C_P and possibly also the optical phonon dispersion. At very high temperatures ($T > 1500$ K) the disagreement with experimental data is natural, since the experimental C_P involves the energy required for the formation of N-vacancies.

4. Conclusion

In summary, we perform systematic first-principles calculations on the structural, electronic, and thermal properties of UN using the LDA/GGA+U method. With the Hubbard U correction, the antiferromagnetic nature of UN is successfully predicted. The atomic structure, including lattice parameters and bulk modulus can be reasonably given, compared with corresponding experimental values. The calculated electronic density of states shows the important role that the 5f electrons play in the conduction band as well as in the valence band. By choosing $U = 2$ eV within GGA, the phonon dispersions and phonon density of states can be reasonably derived with regard to the experimental data. Generally, the calculated specific heat for constant pressure C_P of UN, including both lattice and conduction electron contributions, agrees with the corresponding experimental value in the temperature domain $T < 1500$ K. However, it can still be further enhanced by considering the electron-phonon interactions and many body effects. We expect that our calculated results will be useful for the application of uranium nitride in the Generation-IV reactor and nuclear industry.

Acknowledgments

This work was supported by NSFC under Grant Nos. 90921003 and 60776063.

References

[1] Proceedings of Global Future Reactor Technologies (Tsukuba, Japan, October 2005).
[2] H.J. Matzke, Diffusion Processes in Nuclear Materials, Elsevier, Amsterdam, 1992.
[3] M.S.S. Brooks, J. Phys. F: Met. Phys. 14 (1984) 639–652.
[4] R.A. Evarestov, M.V. Losev, A.I. Panin, N.S. Mosyagin, A.V. Titov, Phys. Stat. Sol. (b) 245 (1) (2008) 114–122.
[5] R.A. Evarestov, A.V. Bandura, M.V. Losev, E.A. Kotomin, YU.F. Zhukovskii, D. Bocharov, J. Comput. Chem. 29 (2008) 2080.
[6] D. Rafaja, L. Havela, R. Ku. el, F. Wastin, E. Colineau, T. Gouder, J. Alloys Compd. 386 (2005) 87–95.
[7] E.A. Kotomin, R.W. Grimes, Y. Mastrikov, N.J. Ashley, J. Phys.: Condens. Matter 19 (2007) 106208.
[8] C.F. van Doorn, P.deV. DuPlessis, J. Magn. Magn. Mater. 5 (1977) 164.
[9] D. Sedmidubsky, R.J.M. Konings, P. Novak, J. Nucl. Mater. 40 (2005) 344.
[10] L. Petit, A. Svane, Z. Szotek, W.M. Temmerman, G.M. Stocks, Phys. Rev. B 80 (2009) 045124.
[11] R. Troć, J. Solid State Chem. 13 (1975) 14.
[12] S.L. Dudarev, G.A. Botton, S.Y. Savrasov, C.J. Humphreys, A.P. Sutton, Phys. Rev. B 57 (1998) 1505.
[13] B. Sun, P. Zhang, X.-G. Zhao, J. Chem. Phys. 128 (2008) 084705.
[14] B.-T. Wang, H. Shi, W.-D. Li, P. Zhang, Phys. Rev. B 81 (2010) 045119.
[15] H. Shi, P. Zhang, S.-S. Li, B. Sun, B. Wang, Phys. Lett. A 373 (2009) 3577.
[16] G. Kresse, J. Furthmller, Computer Code VASP, Vienna, 2005.
[17] G. Kresse, J. Furthmller, Phys. Rev. B 54 (1996) 11169.
[18] P.E. Blöchl, Phys. Rev. B 50 (1994) 17953.
[19] W. Kohn, L.J. Sham, Phys. Rev. 140 (1965) A1133.
[20] J.P. Perdew, K. Burke, Y. Wang, Phys. Rev. B 54 (1996) 16533.
[21] H.J. Monkhorst, J.D. Pack, Phys. Rev. B 13 (1976) 5188.
[22] P. Larson, W.R.L. Lambrecht, A. Chantis, M. van Schilfgaarde, Phys. Rev. B 75 (2007) 045114.
[23] G. Jomard, B. Amadon, F. Bottin, M. Torrent, Phys. Rev. B 78 (2008) 075125.
[24] Boris Dorado, Bernard Amadon, Michel Freyss, Marjorie Bertolus, Phys. Rev. B 79 (2009) 235125.
[25] A. Kotani, T. Yamazaki, Prog. Theor. Phys. 108 (Suppl.) (1992) 117.
[26] F. Brich, Phys. Rev. 71 (1947) 809.
[27] J.A.C. Maples, C.F. Sampson, F.A. Wedgwood, M. Kuznietz, J. Phys. C 8 (1975) 708.
[28] H.J. Matzke, Science of Advanced LMFBR Fuels, North-Holland, Amsterdam, 1986.
[29] J.S. Olsen, L. Gerward, U. Benedict, J. Appl. Crystallogr. 18 (1985) 37.
[30] T.M. Holden, W.J.L. Buyers, C. Svensson, Phys. Rev. B 30 (1984) 114.
[31] P.R. Norton, R.L. Tapping, D.K. Creber, W.J.L. Buyers, Phys. Rev. B. 21 (1980) 6.
[32] R. Bader, Atoms in Molecules: A Quantum Theory, Oxford University Press, New York, 1990.
[33] E.A. Kotomin, R.W. Grimes, Y. Mastrikov, N.J. Ashley, J. Phys.: Condens. Matter 19 (2007) 106208.
[34] K. Parlinski, Z.Q. Li, Y. Kawazone, Phys. Rev. Lett 78 (1997) 4063.
[35] J.A. Jackman, T.M. Holden, W.J.L. Buyers, P.de V. DuPlessis, O. Vogt, J. Genossar, Phys. Rev. B 33 (1986) 10.
[36] J.F. Counsell, R.M. Dell, J.F. Martin, Trans. Faraday Soc. 62 (1966).
[37] C. Affortit, High Temp.–High Press. 1 (1969) 27.
[38] C. Affortit, J. Nucl. Mater. 34 (1970) 105.
[39] F. Oetting, J.M. Leitnaker, J. Chem. Thermodyn. 4 (1972) 199.
[40] H. Tagawa, J. Nucl. Mater. 51 (1974) 78.
[41] T. Matsui, R.W. Ohse, High Temp.–High Press. 19 (1987) 1.
[42] P.-Y. Chevalier, E. Fischer, B. Cheynet, J. Nucl. Mater. 280 (2000) 136–150.
[43] P.F. Weck, E. Kim, N. Balakrishnan, F. Poineau, C.B. Yeamans, K.R. Czerwinski, Chem. Phys. Lett. 443 (2007) 82–86.